Stochastic Nonlinear analysis of vibration based MEMS Piezoelectric Harvesters

H. Madinei, H. Haddad Khodaparast, M. I. Friswell, S. Adhikari

College of Engineering, Swansea University, Bay Campus, Fabian Way, Crymlyn Burrows, Swansea, SA1 8EN, United Kingdom

Abstract

This paper investigates the use of an electrostatic device to improve the performance of MEMS piezoelectric harvesters in the presence of manufacturing uncertainties. Different type of uncertain parameters including thickness, air gap and Young's modulus has been considered. It is shown that existing uncertainty in the geometric and structural parameters of a harvester, can change the resonance frequency and consequently results in a lower output power from the harvesters designed for a nominal excitation frequency. The experimental data from the literature is used to model the uncertainty in the analytical model of the harvester and Monte Carlo Simulation (MCS) is used for uncertainty propagation. It is found that the uncertainty effects can results in two sets of samples. The first set of samples are those with resonance frequency higher than nominal values and the second set includes samples having resonance frequencies lower than nominal value. This paper demonstrates the use of an electrostatic device that can compensate the effects of variability in the harvester by tuning the resonance frequency to the nominal design. The proposed device composes of a symmetric arrangement of two electrodes to decrease the resonance frequency from its nominal value. However, achieving a very good symmetric conditions in the device in the micro-scale is not feasible and therefore the effects of unsymmetric arrangement due to manufacturing variability is investigated. On the other hand, the device includes two arch shape electrodes which can be used to create a hardening effect to increase the resonance frequency of samples which have resonance frequencies smaller than the nominal value.

Keywords: Uncertainty; MEMS; Energy harvester; Piezoelectric

1. Introduction

Harvesting energy from a variety of ambient energy sources (e.g. solar, wind and vibration) is one of the promising ways to provide power for Micro Electro Mechanical Systems (MEMS) in different applications ranging from wireless sensor networks to medical implants [1-4]. Using vibration source has gained more popularity due to its high availability in various environments. There are different transduction methods that can be used to convert mechanical vibrations into electrical energy. The most common types of transduction mechanisms are electrostatic, electromagnetic and piezoelectric. Electrostatic energy harvesters can convert ambient vibrations

to the electrical energy using a charged variable capacitor which its capacitance changes due to the mechanical vibrations. Any change in the capacitance results in a charge rearrangement on the electrodes of the capacitor and consequently the charge flows through the electrical circuit [5]. Electromagnetic vibration based energy harvesters usually consist of a coli, permanent magnet and a suspension spring. According to the Faraday law of electromagnetic induction, when the coil experiences a change in the magnetic flux because of a relative motion between the magnet and the coil, electrical energy is generated [6]. In piezoelectric energy harvesters, the mechanical energy of vibrations is transformed by a piezoelectric material to electrical energy. When a piezoelectric material is deformed, the central molecules in the crystal become polarized and form a dipole. If the dipoles are arranged, then two surfaces of the material become positively and negatively charged [7]. Due to the compatibility between piezoelectric material deposition and MEMS fabrication process, piezoelectric convertors have been recognized to offer more benefits [8].

Generally, in vibration based energy harvesters (VEHs) the maximum energy can be harvested when the harvester excited at its resonance frequency. In most cases the resonance frequency of the harvester dose not match the frequency of vibration source and consequently the output power decreases significantly. There are two methods to increase the efficiency of the VEHs: broadening the bandwidth and tuning the resonance frequency of the harvester [9-10].

In the last few years, many studies focused on these methods to improve the harvested power of VEHs. Masana and Daqaq [11] developed an electromechanical nonlinear model of an axially loaded, tunable, and couple clamped end energy harvesting beam. They illustrated that the axial static load can be used to tune the system over a wide range of frequency. Challa et al. [12] investigated a vibration energy harvesting device with autonomously tunable resonance frequency. They used a piezoelectric cantilever beam array with magnets attached to the free ends of cantilever beams to tune resonance frequency of the system by magnetic force. Miller et al. [13] proposed a passive self-tuning beam resonator with sliding proof mass along the beam. This model enables the energy harvesting system to adjust the natural frequency of the system and thereby increase the energy harvested over time. Erturk and Inman [14] investigated the broadband high-energy orbits in a bistable piezomagnetoelastic energy harvester over a range of excitation frequency. Malaji and Faruque Ali [15] analysed broadband energy harvesting using multiple linear harvesters. They showed that bandwidth of harvesting frequency can be increased by using an array of coupled pendulums with mechanical grounding. In addition, they found that the bandwidth and the total harvested power saturates with the number of pendulums.

A mismatch between the resonance frequency and vibration source frequency may exist either due to changes in the working conditions or excessive manufacturing tolerances and errors. In MEMS devices due to the fabrication process such as mask alignment, deposition, photolithography, etching and drying, manufacturing tolerances are generally high and in some cases it can be higher than ±10% of nominal values [16]. Therefore, parameter uncertainty can significantly affect the performance of MEMS devices. Uncertainty analysis of MEMS devices has been studied by several authors in the literature. Agarwal and Aluru [17] presented a framework to quantify

different kind of outputs in MEMS structure such as deformation and electrostatic pressure in these devices. Agarwal and Aluru [18] proposed a framework to include the effect of uncertain design parameters of MEMS devices. Based on this framework they investigated the effect of variations in Young's modulus, induced because of variations in manufacturing process parameters or heterogeneous measurements, on the performance of a MEMS switch.

In this paper, an electrostatic device has been proposed to compensate the effect of manufacturing uncertainties on performance of MEMS piezoelectric harvesters. In this model, the resonance frequency of harvester is tuned using an arch electrode and two straight electrodes. The manufacturing uncertainty could potentially change the harvester's resonance frequency and consequently the direction of the deviation from its nominal value may be positive or negative. Therefore, there is a need for tuning the harvester's resonance frequency to a higher (hardening) or lower (softening). Based on applying voltage to the aforementioned electrodes, the resonance frequency of harvester can be adjusted through hardening and softening mechanisms. Applying DC voltage to the arch shaped electrode creates a tensile follower force which can increase the resonance frequency of harvester linearly. On the other hand, the resonance frequency of harvester can be decreased by applying voltage to the straight electrodes which creates a softening nonlinearity. The Galerkin method has been used to discretised the equations of motion. To show the results, a single mode approximation of the harvester has been considered. Due to the nonlinearity of the electrostatic force, finding the analytical solution for the derived equations is challenging. Therefore, in this work shooting method has been used to solve the derived equations. By considering 2000 samples, the distribution of the resonance frequency and harvested power of samples have been estimated using MCS in presence of structural uncertainty.

2. Model description and mathematical modeling

Figure 1 shows the proposed model in this paper. The model is an isotropic micro-beam of length L, width a, thickness h, density ρ and Young's modulus E, sandwiched with piezoceramic layers having thickness h_0, Young's modulus E_0 and density ρ_0 throughout the micro-beam length and located between two straight-shaped electrodes and one arc-shaped electrode. As illustrated in Figure 1, the piezoceramic layers are connected to the resistance (R) and the coordinate system is attached to the middle of the left end of the micro-beam where x and z refer to the horizontal and vertical coordinates respectively. The free end of the micro-beam is attached to the two arc-shaped comb fingers which subtend angle α at the base of the beam and remain parallel to the fixed arc-shaped electrode. The governing equation of transverse motion can be written as [19]

$$\begin{aligned}&\frac{\partial^2}{\partial\hat{x}^2}\left(EI\left(\hat{x},\hat{\psi}\right)\frac{\partial^2\hat{w}}{\partial\hat{x}^2}\right)+\ \rho A\left(\hat{x},\hat{\psi}\right)\frac{\partial^2\hat{w}}{\partial\hat{t}^2}+\hat{c}_a\frac{\partial\hat{w}}{\partial\hat{t}}+F_f\left(\hat{\psi}\right)\frac{\partial^2\hat{w}}{\partial\hat{x}^2}\\&-\hat{\vartheta}\left(\hat{\psi}\right)v(\hat{t})\left(\frac{d\delta(\hat{x})}{d\hat{x}}-\frac{d\delta(\hat{x}-L_c)}{d\hat{x}}\right)=F_e\left(\hat{\psi}\right)+z_0\hat{\Omega}^2\left(\rho A\left(\hat{x},\hat{\psi}\right)+M_t\delta(\hat{x}-L)\right)\cos\left(\hat{\Omega}\hat{t}\right)\end{aligned}\tag{1}$$

and subjected to the following boundary conditions

$$\widehat{w}(0,\hat{t}) = 0 \quad \frac{\partial \widehat{w}(0,\hat{t})}{\partial \hat{x}} = 0$$
$$\frac{\partial}{\partial \hat{x}}\left(EI(\hat{x},\widehat{\psi})\frac{\partial^2 \widehat{w}(L,\hat{t})}{\partial \hat{x}^2}\right) = M_t\left(\frac{\partial^2 \widehat{w}(L,\hat{t})}{\partial \hat{t}^2}\right) \tag{2}$$
$$\frac{\partial^2 \widehat{w}(L,\hat{t})}{\partial \hat{x}^2} = 0$$

where $\widehat{\psi}$ shows the stochastic parameters, which have been used as an input to the mathematical model.

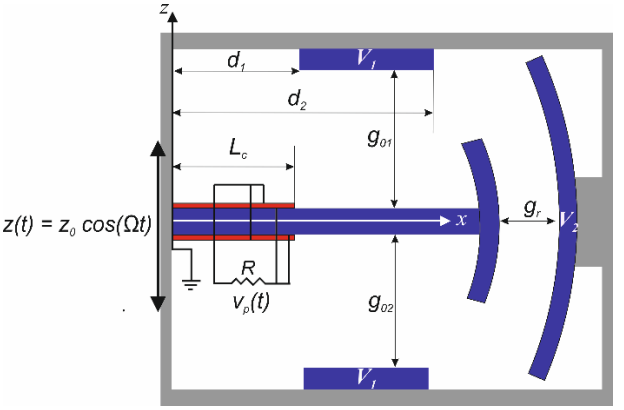

Fig. 1. Schematic of the proposed energy harvester

In Equation (1), $\widehat{w}$ is the transverse deflection of the beam relative to its base at the position $\hat{x}$ and time $\hat{t}$, c_a is the viscous air damping coefficient, $\delta(\hat{x})$ is the Dirac delta function, $z(\hat{t})$ is the base excitation function, F_f is the follower force which is applied to the harvester by the arched-shaped electrode, F_e is the electrostatic force which is applied to the harvester by the straight-shaped electrodes, $v(\hat{t})$ is the voltage across the electrodes of each piezoceramic layer, $\hat{\vartheta}$ is the coupling term which is dependent on the type of connection between the piezoceramic layers (i.e. series or parallel connections). By considering the parallel connection between these layers and Kirchhoff's laws, the electrical circuit equation can be expressed as

$$C_p(\widehat{\psi})\frac{dv_p(\hat{t})}{d\hat{t}} + \frac{v_p(\hat{t})}{2R} + i_p(\hat{t},\widehat{\psi}) = 0 \tag{3}$$

where the internal capacitance (C_p), coupling term (θ_p) and the current source can be obtained as [19]

$$C_p(\widehat{\psi}) = \frac{\bar{\varepsilon}_{33}^{s} a L_c}{h_0}, \qquad \hat{\vartheta}_p(\widehat{\psi}) = \frac{\bar{e}_{31} a}{h_0}\left(\left(h_0 + \frac{h}{2}\right)^2 - \frac{h^2}{4}\right), \tag{4}$$

$$i_p(\hat{t},\hat{\psi}) = \frac{\bar{e}_{31}a}{2}(h_0+h)\int_0^{L_c}\frac{\partial^3\hat{w}(\hat{x},\hat{t})}{\partial\hat{x}^2\partial\hat{t}}d\hat{x}$$

and $\bar{\varepsilon}_{33}^{S}$ is the permittivity component at constant strain with the plane stress assumption for the beam. Using electrostatic principles, the electrostatic force between the micro-beam and the straight electrodes (F_e) can be written as [20]

$$F_e(\hat{\psi}) = \frac{\varepsilon_0 a\, H(\hat{x})}{2}\left(\frac{V_1^2}{(g_{01}-\hat{w})^2}-\frac{V_1^2}{(g_{02}+\hat{w})^2}\right) \tag{5}$$

where

$$H(\hat{x}) = H(\hat{x}-\hat{d}_1) - H(\hat{x}-\hat{d}_2) \tag{6}$$

In Equation (5), ε_0 is the permittivity of free space, $H(\hat{x})$ is the Heaviside function, V_1 is the applied DC voltage to the straight electrodes, g_{01} and g_{02} are the air gaps between the micro-beam and the straight electrodes. By applying voltage to the arched-shaped electrode shown in Figure 1, the amplitude of F_f can be tuned. Figure 3 shows for a small angular deflection of the micro-beam (θ), the angular overlap between the fingers and the arched-shaped electrode is always 2α and the force remains a follower force in all conditions.

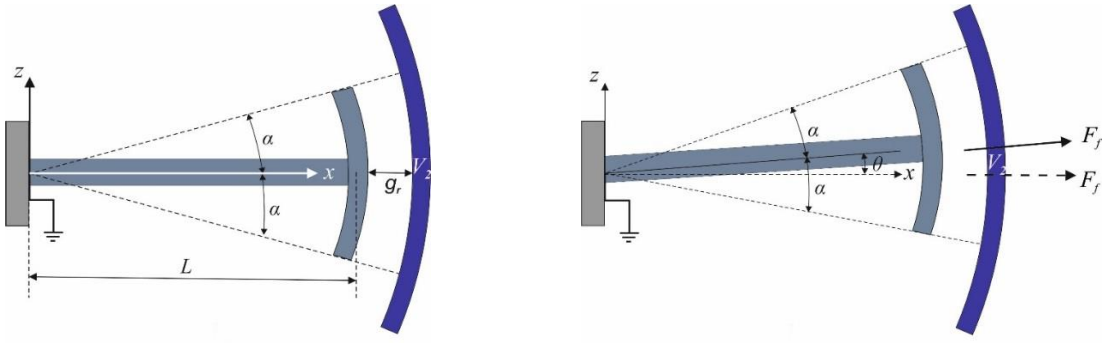

(a) (b)

Figure 3: A micro-beam with an arc-shaped comb fingers in its (a) unperturbed state and (b) perturbed state.

Based on electrostatic principles, the amplitude of the follower force (F_f) can be written as

$$F_f(\hat{\psi}) = \frac{\varepsilon_0 a}{g_r^2}\, V_2^2 L\alpha \tag{7}$$

where g_r is the radial gap between the comb fingers and arched-shaped electrode, a is the width of the resonator, L is the length of the beam (the thickness of the arched-shaped electrode can be ignored), and V_2 is the applied voltage to the arched-shaped electrode. For convenience, Equations (1) and (3) can be rewritten in a non-dimensional form as follows

$$\frac{\partial^2}{\partial x^2}\left(s_1(x,\psi)\frac{\partial^2 w}{\partial x^2}\right)+s_2(x,\psi)\frac{\partial^2 w}{\partial t^2}+c_a\frac{\partial w}{\partial t}$$

$$+\left(\alpha_f(\psi)\,V_2^2\right)\frac{\partial^2 w}{\partial x^2}-\vartheta_p(\psi)\,v_p(t)\left(\frac{d\delta(x)}{dx}-\frac{d\delta(x-l_c)}{dx}\right) \tag{8}$$

$$=\alpha_e(\psi)\,V_1^2\left(\frac{H(x)}{(1-w)^2}-\frac{H(x)}{(r(\psi)+w)^2}\right)+\left(\sigma_1 s_2(x,\psi)+\sigma_2\delta(x-1)\right)\Omega^2\cos(\Omega t)$$

$$\frac{dv_p(t)}{dt}+\lambda(\psi)\,v_p(t)+\gamma(\psi)\int_0^{l_c}\frac{\partial^3 w}{\partial x^2\partial t}dx=0 \tag{9}$$

where

$$w=\frac{\widehat{w}}{g_{01}} \qquad x=\frac{\hat{x}}{L} \qquad t=\frac{\hat{t}}{T}, \qquad \Omega=T\hat{\Omega}, \qquad l_c=\frac{L_c}{L}$$

$$c_a=\frac{\hat{c}_a L^4}{(EI)_C\,T}, \qquad T=\sqrt{\frac{(\rho A)_C L^4}{(EI)_C}}, \qquad \vartheta_p=\frac{\hat{\vartheta}_p L^2}{(EI)_C g_{01}}, \qquad \alpha_f=\frac{\varepsilon_0 a L^3\alpha}{(EI)_C g_r^2}$$

$$\alpha_e=\frac{\varepsilon_0 a L^4}{2g_{01}^3(EI)_C}, \qquad \sigma_1=\frac{z_0 L^4\,(\rho A)_C}{T^2(EI)_C g_{01}}, \qquad \sigma_2=\frac{z_0 L^3 M_t}{T^2(EI)_C g_{01}}, \qquad \lambda=\frac{T}{2RC_p}, \tag{10}$$

$$\gamma=\frac{\bar{e}_{31} a g_{01}(h_0+h)}{2C_p L}, \qquad r=\frac{g_{02}}{g_{01}}, \qquad s_1=\frac{EI(\hat{x},\psi)}{(EI)_C}, \quad s_2=\frac{\rho A(\hat{x},\psi)}{(\rho A)_C}$$

where $(EI)_C$ and $(\rho A)_C$ are related to the bimorph part of the beam. To eliminate the spatial dependence in Equations (8) and (9) the Galerkin decomposition method is used. The deflection of the micro-beam can be represented as a series expansion in terms of the eigenfunctions of the micro-beam, i.e.

$$w(x,t)=\sum_{i=1}^{N}U_i(t)\varphi_i(x) \tag{11}$$

where $\varphi_i(x)$ is the *i*th linear undamped mode shape of the straight micro-beam and $U_i(t)$ is the *i*th generalized coordinate. Equations (8) and (9) can be converted into a system of differential equations using this method. A single-mode approximation yields the following equations

$$\ddot{U}(t)+2\mu\omega_n\,\dot{U}(t)+\omega_n^2 U(t)-\theta_p\,v_p(t)=\alpha_t\int_0^1\left(\frac{V_1^2 H(x)}{(1-U\varphi)^2}-\frac{V_1^2 H(x)}{(r+U\varphi)^2}\right)\varphi\,dx$$
$$+F\,\Omega^2\cos(\Omega t) \tag{12}$$

$$\dot{v}_p(t)+\lambda\,v_p(t)+\beta\,\dot{U}(t)=0 \tag{13}$$

where

$$M = \int_0^1 s_2(x,\psi)\,\varphi^2(x)\,dx,\;\; C = c_a \int_0^1 \varphi^2(x)\,dx,\;\; K_f = \alpha_f\, V_2^2 \int_0^1 \varphi(x)\,\varphi^{II}(x)dx,$$
$$K_m = \int_0^1 \left(s_1{}^{II}(x,\psi)\varphi^{II}(x) + 2s_1{}^{I}(x,\psi)\varphi^{III}(x) + s_1(x,\psi)\varphi^{IV}(x)\right)\varphi(x)\,dx,$$
$$F = \frac{1}{M}\left(\sigma_1 \int_0^1 \varphi(x) s_2(x,\psi)\,dx + \sigma_2 \int_0^1 \varphi(x)\,\delta(x-1)dx\right), \qquad \alpha_t = \frac{\alpha_e}{M}, \tag{14}$$
$$\beta = \gamma\left(\frac{d\varphi(l_c)}{dx}\right), \qquad \mu = \frac{C}{2M\omega_n}, \qquad \omega_n = \sqrt{\frac{K_m + K_f}{M}}, \qquad \theta_p = \frac{\vartheta_p}{M}\left(\frac{d\varphi(l_c)}{dx}\right)$$

Due to the electrostatic nonlinearity in Equation (8), finding an analytical solution to study the dynamic behavior of the system is quite complicated. However, there are different methods to find an approximated analytical solution of Equations (8) and (9). Previously the authors (Madinei et al. [21]) used harmonic balance method to study the dynamic behavior of the system by considering approximated electrostatic force using Taylor expansion. They assumed symmetric electrostatic force in their approximation and showed that acceptable convergence can be obtained by including the terms up to ninth-order. However, in the presence of manufacturing uncertainties the electrostatic force could be unsymmetric due to the variabilities in the air gap and more terms may be needed to be included to reach acceptable convergence. Therefore, using harmonic balance method makes the uncertainty propagation tedious because for every different sample, the number of truncated terms should be determined. In current work, shooting method [22] is used to study the dynamic behavior of the system. Generally, the shooting method is a powerful and useful method to find periodic solutions of a nonlinear system, and it is computationally more time efficient than direct integration methods. The method can also find the unstable solutions although this is not needed for the analysis in this paper. By introducing $X_1 = U, X_2 = \dot{U}$ and $X_3 = v_p$, Equations (12) and (13) can be rewritten as

$$\dot{X}_1 = X_2, \tag{15}$$
$$\dot{X}_2 = F\cos(\Omega t) - 2\mu\omega_n X_2 - \omega_n^2 X_1 + \theta_p X_3 + \alpha_t\, V_1^2 \int_0^1 \left(\frac{H(x)}{(1-X_1\varphi)^2} - \frac{H(x)}{(r+X_1\varphi)^2}\right)\varphi\, dx \tag{16}$$
$$\dot{X}_3 = -\lambda\, X_3 - \beta\, X_2 \tag{17}$$

To find the periodic solution of Equations (15), (16) and (17), we need to search for an appropriate set of initial condition (η_1, η_2, η_3). To proceed with the shooting technique, for convenience, we define the following variables

$$X_4 = \frac{\partial X_1}{\partial \eta_1}, \qquad X_5 = \frac{\partial X_1}{\partial \eta_2}, \qquad X_6 = \frac{\partial X_1}{\partial \eta_3}$$
$$X_7 = \frac{\partial X_2}{\partial \eta_1}, \qquad X_8 = \frac{\partial X_2}{\partial \eta_2}, \qquad X_9 = \frac{\partial X_2}{\partial \eta_3} \tag{18}$$
$$X_{10} = \frac{\partial X_3}{\partial \eta_1}, \qquad X_{11} = \frac{\partial X_3}{\partial \eta_2}, \qquad X_{12} = \frac{\partial X_3}{\partial \eta_3}$$

The shooting technique requires simultaneously integrating Equations (15), (16) and (17) plus the time derivatives of the variables $(\dot{X}_4 - \dot{X}_{12})$ in time domain for one period of excitation. The initial conditions for solving the set of differential equations are defined as

$$\begin{aligned} &X_1(0) = \eta_{10}, \quad X_2(0) = \eta_{20}, \quad X_3(0) = \eta_{30}, \quad X_4(0) = 1, \quad X_5(0) = 0, \\ &X_6(0) = 0, \quad X_7(0) = 0, \quad X_8(0) = 1, \quad X_9(0) = 0, \quad X_{10}(0) = 0, \\ &X_{11}(0) = 0, \quad X_{12}(0) = 1 \end{aligned} \tag{19}$$

η_{10}, η_{20} and η_{30} are initial guesses for the initial condition that result in periodic solution. Generally, these initial guesses deviate from the exact one by an error or correction $\delta\boldsymbol{\eta}$. By calculating the values of $X_4 - X_{12}$ at one-period and substituting them in the below algebraic system of equations the error can be found for each set of initial guesses [22].

$$\left[\begin{bmatrix} X_4 & X_5 & X_6 \\ X_7 & X_8 & X_9 \\ X_{10} & X_{11} & X_{12} \end{bmatrix} - [I]\right]\begin{bmatrix} \delta\eta_1 \\ \delta\eta_2 \\ \delta\eta_3 \end{bmatrix} = \begin{bmatrix} \eta_{10} - X_1(T, \eta_{10}, \eta_{20}, \eta_{30}) \\ \eta_{20} - X_2(T, \eta_{10}, \eta_{20}, \eta_{30}) \\ \eta_{30} - X_3(T, \eta_{10}, \eta_{20}, \eta_{30}) \end{bmatrix} \tag{20}$$

By trying different initial guesses and using Equation (20), the error ($\delta\eta_1, \delta\eta_2$ and $\delta\eta_3$) can be minimized and a convergence is achieved. Then, the peak power through the resistance can be obtained by substituting v_p into the following equation

$$P_0 = \frac{{v_p}^2}{R} \tag{21}$$

3. Numerical Results and Discussion

To demonstrate the results of analysis presented in the previous section, a bimorph piezoelectric micro cantilever beam is considered with the geometrical and material properties as listed in Table 1.

Table 1. Geometrical and material properties of the harvester.

Length, L (μm)	3000
Width, a (μm)	1000
Thickness, h (μm)	4
Thickness, h_0 (μm)	2
Young's modulus, E (GPa)	169.6
Young's modulus, E_0 (GPa)	65
Air gap, g_0 (μm)	40
Air gap, g_r (μm)	3
Damping coefficient, c_a(N.s/m)	0.002
Density of Si beam, ρ (kg/m^3)	2330
Density of PZT, ρ_0(kg/m^3)	7800
Equivalent piezoelectric coefficient, $\bar{e}_{31}$(Cm^{-2})	-11.18
Permittivity component, $\bar{\varepsilon}_{33}^{s}$(nF/m)	13.48

Based on the experimental results [16], the most important variations of the fabrication parameters include thickness, air gap and Young's modulus. To show the effect of these parameters on the performance of the harvester, a Gaussian distribution of parameters are assumed [16] and given in Table 2.

Table 2. Most sensitive parameters to manufacturing uncertainties [16].

Data	Mean	Std	COV (%)
Thickness, h (μm)	4	0.35	8.75
Thickness, h_0 (μm)	2	0.175	8.75
Young's modulus, E (GPa)	169.6	16.58	9.78
Young's modulus, E_0 (GPa)	65	6.35	9.78
Air gap, g_0 (μm)	40	2.52	6.3
Air gap, g_r (μm)	3	0.18	6.3

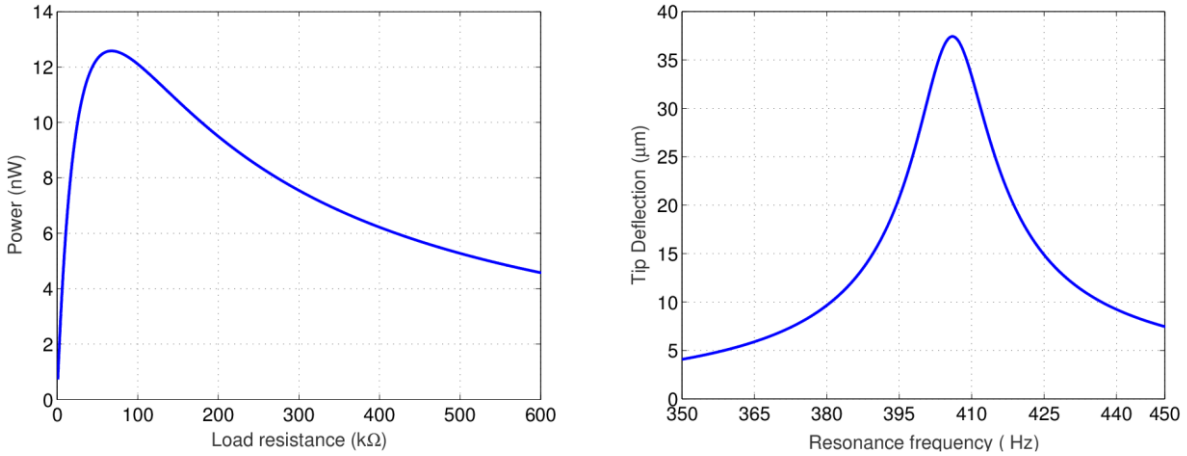

(a) (b)

Figure 4: (a)Variation of the piezoelectric peak power with load resistance at nominal resonance frequency (b) Displacement frequency response curve with the optimal resistance

Considering the mean parameters of the micro beam, the optimal resistance of the harvester is obtained at its resonance frequency. As shown in Figure 4a, by exciting harvester at its resonance frequency, 12.6 nW power can be harvested at the optimal resistance. To investigate the effect of the manufacturing uncertainties on the performance of the MEMS piezoelectric harvester, different number of samples are generated and the Monte Carlo simulation is used for uncertainty propagation. Figure 5a shows that the Probability density function (PDF) of the power do not significantly change when the number of samples increased from 1500 to 2000, hence 2000 samples will be enough for uncertainty analysis.

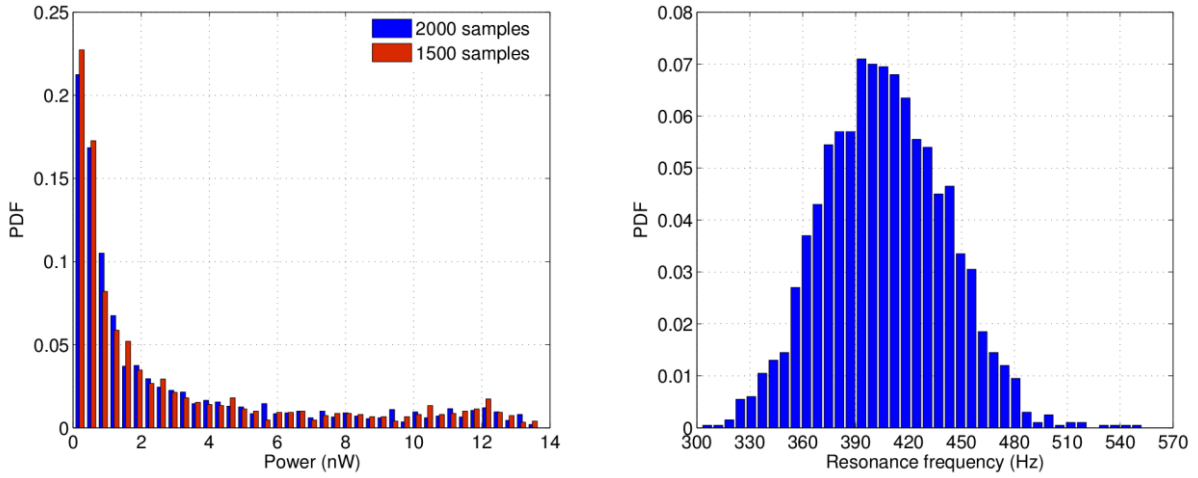

(a) (b)

Figure 5: Probability density function of (a) resonance frequency and (b) harvested power.

Due to the variability of the parameters, the resonance frequencies of the samples have a large deviation from one sample to another and this can significantly decrease the performance of the harvester. Figure 5b shows that the mean resonance frequency of the harvester is 406 Hz, however there are many samples which have resonance frequencies either greater or less than the mean value. On the other hand, because of this variability in resonance frequency, the harvested power of most samples are far away from the power of the system with the mean parameters when it is excited by mean/nominal resonance frequency (see Figure 5a). In order to compensate the effect of manufacturing uncertainties, the resonance frequency of samples can be adjusted by applying voltage to the electrodes. Figure 6a shows that by applying voltage to the straight electrodes, the resonance frequency of micro-beam decreases due to the softening nonlinearity of the electrostatic field. Considering this nonlinearity, there are multiple solutions for the micro beam response within the frequency range close to the frequency of vibration source. In order to harvest more power, the micro beam response should be at the higher of the two solutions and close to the resonance frequency. However, being at the higher solution depends on the initial conditions and therefore the response at the higher amplitude cannot be guaranteed. Using the applied DC voltage can ensure the response of the harvester to be in the higher solution. For a given excitation frequency if the harvester response happens to be in the lower amplitude solution the DC voltage is increased until a region is reached where the harvester only has a single solution. The DC voltage is then slowly reduced and the harvester follows high amplitude solution until the resonance is obtained.

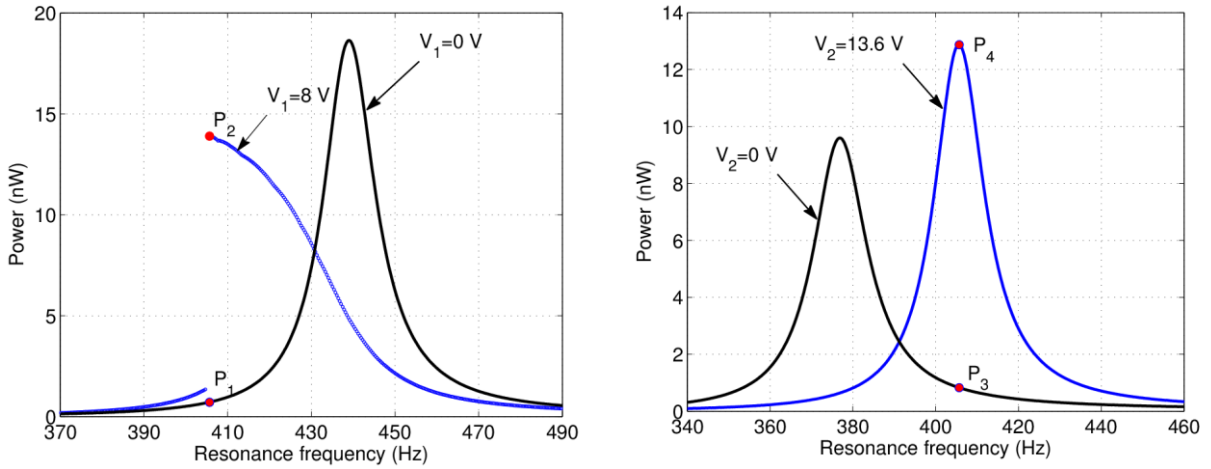

(a) (b)

Figure 6: Tuning resonance frequency of micro beam using (a) softening ($d_2 - d_1 = 0.5L$) and (b) hardening ($\alpha = 30^{\circ}$) mechanism

As shown in Figure 6a, by applying 8 V to the electrodes, the resonance frequency of the sample is decreased by 7.5 percentage to match the frequency of vibration source. Consequently, the harvested power can be increased by 13.2 nW. On the other hand, Figure 6b shows that the resonance frequency of micro beam can be increased by applying a follower force. In Figure 6b, an arbitrary sample with resonance frequency less than 406 Hz has been considered. Using hardening mechanism and applying 13.6 V, the resonance frequency of the sample can be increased by 7.7 percentage and therefore more power can be harvested.

In both mechanisms, the resonance frequency of sample is tuned based on the electrostatic force. The magnitude of this force can be controlled by voltage, air gap and overlapping area between electrodes. Generally, the air gap and overlapping area is considered as designed parameters and they are constant. However, based on Table 2, the air gaps between electrodes will be affected by manufacturing uncertainties. Therefore, depending on the air gaps between electrodes, the resonance frequency of sample can be tuned by applied DC voltage. In hardening mechanism, by applying voltage to the arch shape electrodes the resonance frequency of the harvester is changed linearly but in the softening mechanism due to the geometric configuration of the electrodes, the behavior of the harvester is affected by electrostatic nonlinearity.

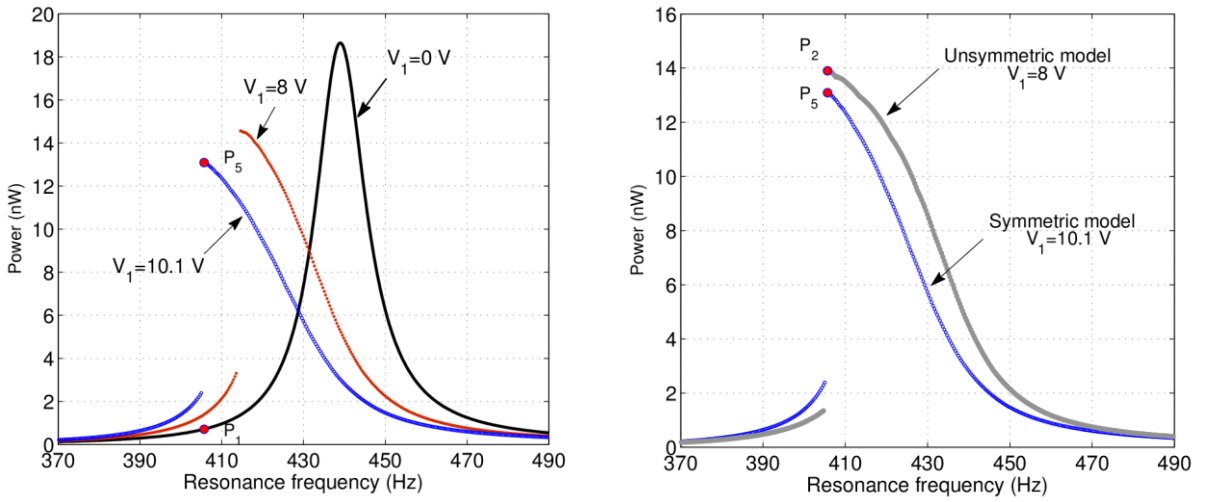

(a) (b)

Figure 7: (a)Tuning resonance frequency of symmetric model ($g_{01} = g_{02} = 40\mu m$) (b) comparison of symmetric and unsymmetric model ($g_{01} = 44.6\mu m,\ g_{02} = 36\mu m$)

In addition, due to the variabilities in the air gap between two straight electrodes the system may become unsymmetric. According to Equation (5), amplitude of the electrostatic force can be controlled by applied DC voltage (V_1) and the air gap between electrodes. As shown in Figure 7a, by considering equal initial gaps between electrodes ($g_{01} = g_{02} = 40\mu m$), the resonance frequency of the sample can be tuned to the nominal frequency by applying 10.1 V to the electrodes. However, by including the variabilities in the air gap, resonance frequency shifting for the same sample can be done by applying 8 V to the electrodes (See Figure 7b). Therefore, in comparison with symmetric model depending on the initial gaps between electrodes in the unsymmetric model, the applied DC voltage may either increased or decreased. In addition, as shown in Figure 8 the steady state response of output power for unsymmetric model can be different in comparison with the symmetric model. In the unsymmetric model due to the nonzero static deflection, the output voltage will be affected by a DC offset. Therefore, the output voltage will be swinged between two different values, instead of usual $+v_{ac}$ V and $-v_{ac}$ V. Consequently, there will be double picks in the steady state response of the output power in the unsymmetric model (see figure 8a).

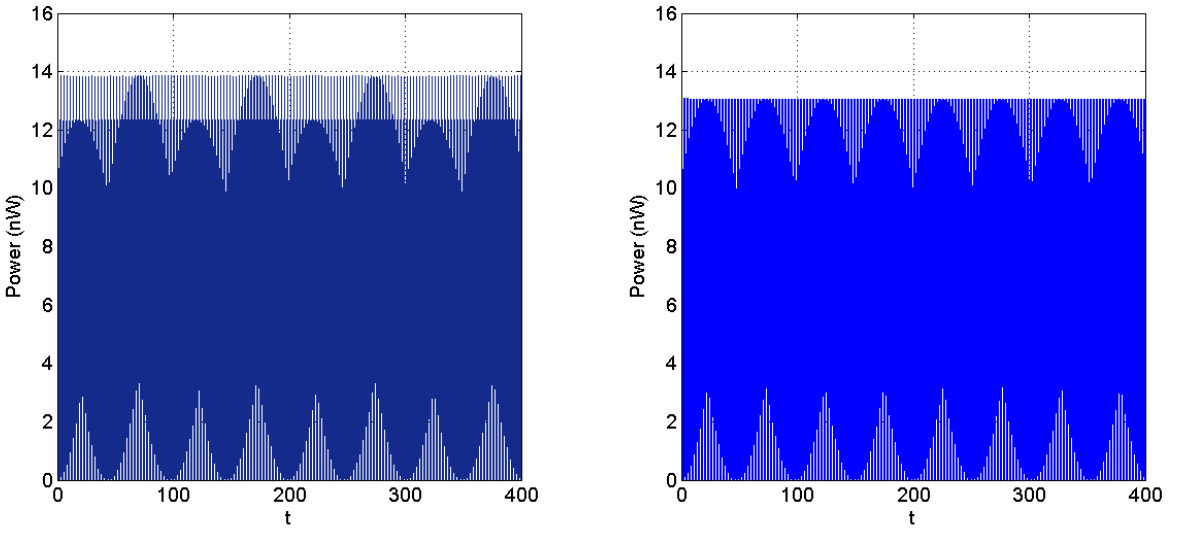

(a) (b)

Figure 8: Steady state response of the output power at 406 Hz (a) unsymmetric model ($V_1 = 8\,V$) (b) symmetric ($V_1 = 10.1\,V$)

Generally, in nonlinear energy harvesters the maximum power can be harvested when the harvester is working at upper branch in vicinity of its resonance frequency. By any changes in the initial condition, the harvester tend to jump down to the lower branch and therefore the harvested power will be decreased significantly. As shown in Figure 9a, by jumping down from point P_2 in Figure 7b the harvested power decreases by 89 percentage.

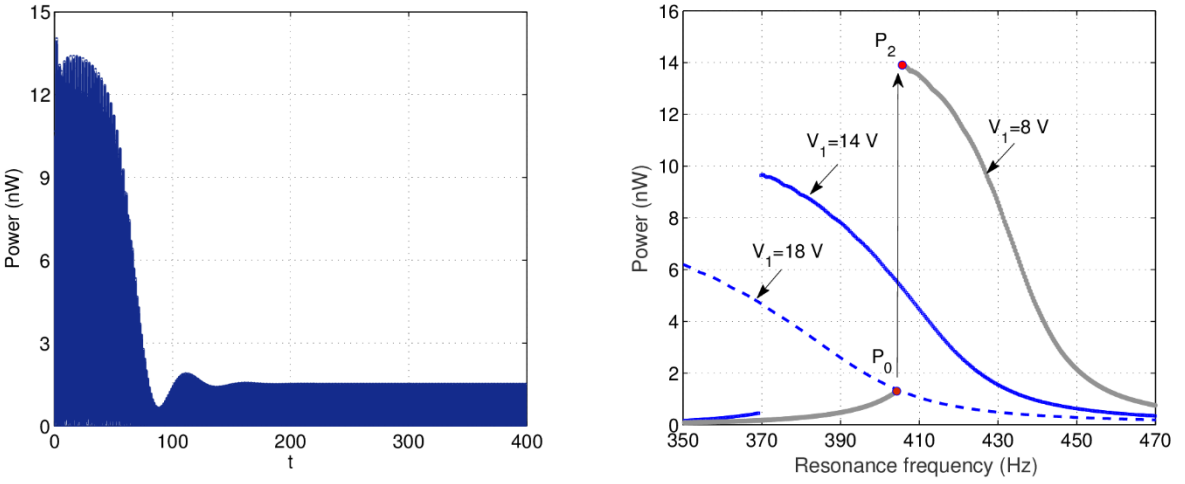

(a) (b)

Figure 9: (a) The output power of the harvester at lower branch ($\Omega = 406\,Hz, V_1 = 8\,V$) (b) Moving from lower branch to higher one by decreasing voltage approach.

Figure 9b shows that in the case of jumping down to the lower solution (P_0), the applied DC voltage is increased until a region is reached where the harvester only has a single solution. Then by delivering a gradually decreasing voltage in the fixed frequency direction the harvester follows high amplitude solution until the resonance is obtained.

The voltage source in both symmetric and unsymmetric models can be charged through the harvested power from the electrostatic side. Generally, electrostatic harvesters require an energy cycle to convert the mechanical energy to the electrical energy [24]. The energy conversion cycles mostly rely on charge or voltage constraint concepts. In both cycles, electrical charge is stored in a variable capacitor when its capacitance is high. Then the capacitance of the capacitor is reduced to the minimal by mechanical vibration, and eventually the capacitor will be discharged. Considering the voltage constraint cycle, as shown in Figure 10a, there are two variable capacitors between beam and straight electrodes. In each cycle of vibration, these capacitors charged and discharged continuously and they can charge the voltage source (V_1) based on the voltage constraint cycle. Therefore, in both symmetric and unsymmetric model the voltage source is self-chargeable and the harvested power from electrostatic side is used to keep the voltage source constant [21].

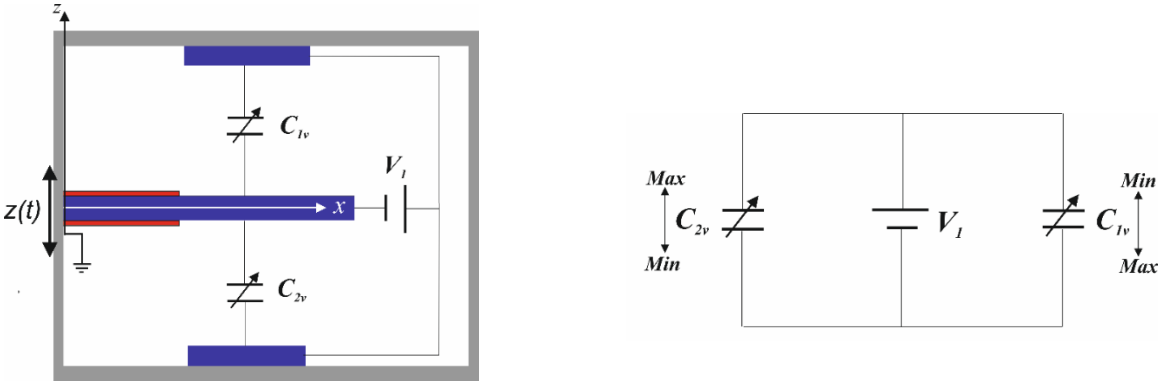

(a) (b)

Figure 10: (a)Variable capacitors in the proposed model (b) Electrical circuit

Considering all samples, the performance of the harvester can be increased by using hardening and softening mechanisms. Figure 11 shows significant increase in the harvested power of samples after using the softening and hardening mechanisms. By applying different voltages to the electrodes, the resonance frequency of the samples matches the excitation frequency and it can harvest more power.

Figure 12 shows that by applying DC voltage to the straight electrodes (V_1) up to 26.6 V and the arch electrodes (V_2) up to 24 V, the harvested power of samples can be improved significantly and consequently, in comparison with Figure 5b, most of samples are shifted to the region around the power of the system with the mean parameters. As shown in Figure 11a the mean applied DC voltage to the straight electrodes (point A) is 8.5 V and in most cases the harvested power of samples is closed to the power of the system with the mean parameters.

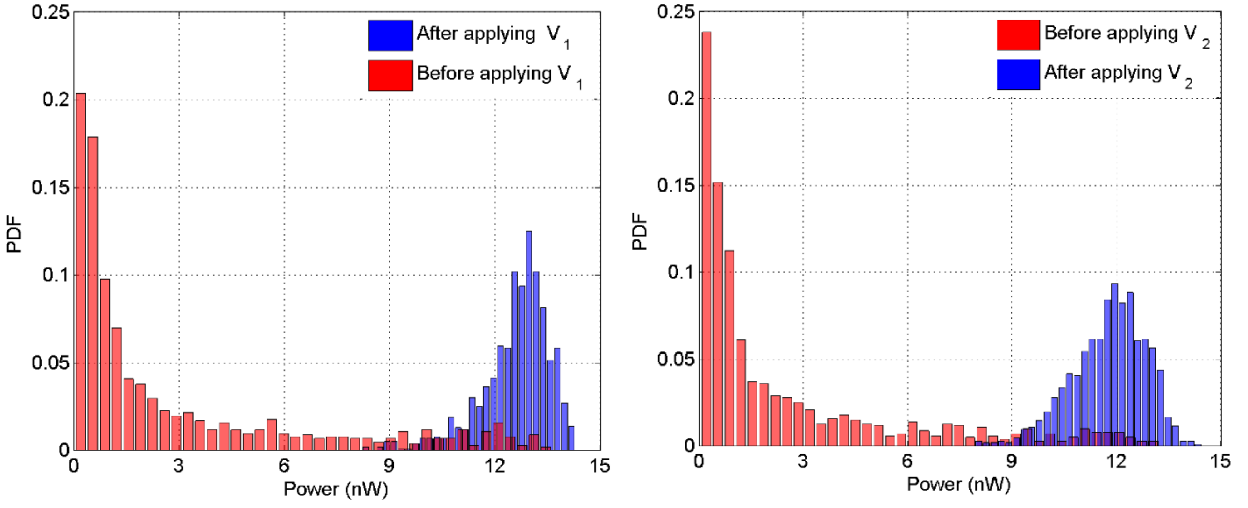

(a) (b)

Figure 11: Harvested power of samples based on (a) softening and (b) hardening mechanism

However, in hardening mechanism, the mean applied DC voltage (point B in figure 10b) is 3.7 V greater than mean applied DC voltage in softening mechanism. Furthermore, the mean harvested power of samples in hardening mechanism is less than 12 nW. Therefore, the electrostatic nonlinearity in the softening mechanism can make the tuning mechanism more efficient in comparison with the hardening mechanism.

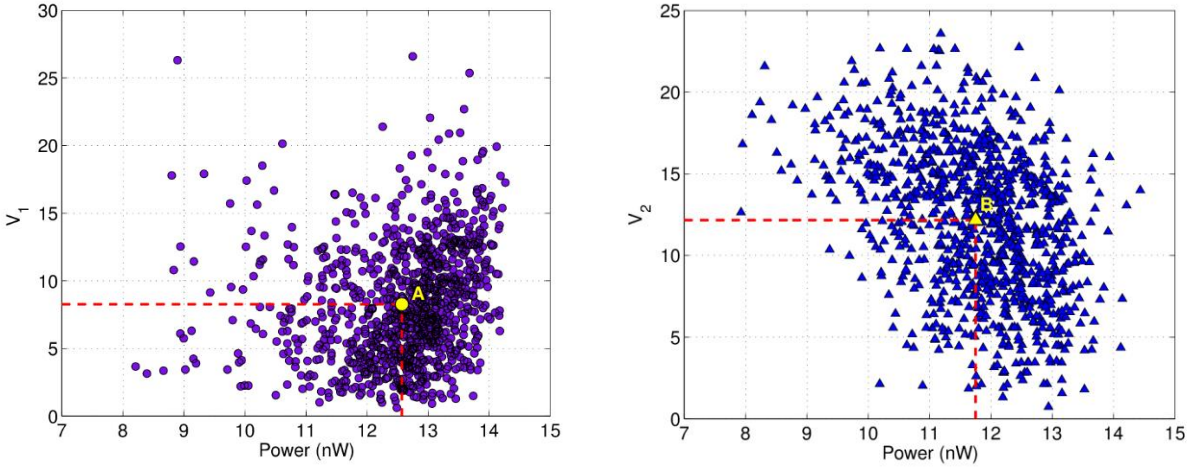

(a) (b)

Figure 12: (a) Applied DC voltage versus harvested power for softening mechanism and (b) hardening mechanism

In the current analysis, a constant optimal resistance (70 kΩ) is used for all samples; however this resistance can be optimized for each sample [21]. In addition, since the axial deflection of the beam is negligible, the power loss of voltage source V_2 is small. Considering the results of both mechanisms, as shown in Figure 13 by using the electrostatic force in both mechanisms the effect

of manufacturing uncertainties can be compensated and after tuning the resonance frequencies of samples, the harvested powers of samples are varied between 8 to 14 nW.

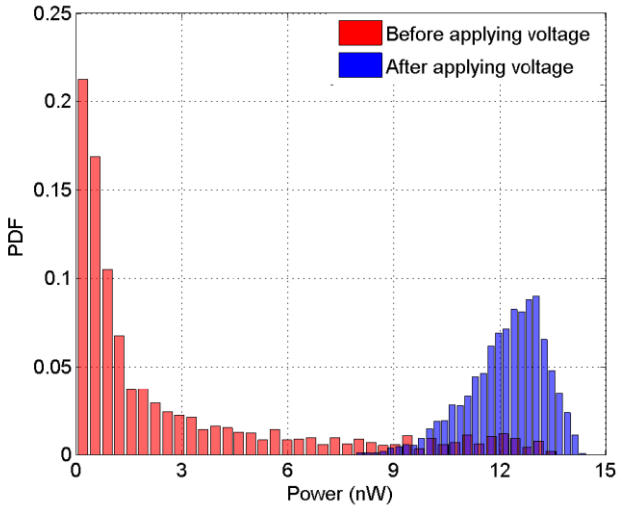

Figure 13: Harvested power of samples before and after applying DC voltage

4. Conclusions

In this paper, the effect of manufacturing uncertainties on the performance of MEMS piezoelectric harvesters was investigated. The steady state solution was obtained by using shooting method and 2,000 samples were considered based on the Monte Carlo simulation. The results showed that due to the variability of parameters, the resonance frequencies of the samples in most cases were far away from the excitation frequency and results in lower harvested power. Two tuning mechanisms were used to compensate the effect of manufacturing uncertainty. Based on these mechanisms, it was observed that the harvested power can be increased by applying DC voltage to the straight electrodes and arch shaped electrode up to 26.6 V and 24 V, respectively. In addition, it was shown that due to the nonlinearity in the softening mechanism, it is more efficient than the hardening one. However, the use of the softening mechanism for all samples requires the resonance frequency of the nominal system to be greater than excitation frequency.

Acknowledgements

Hadi Madinei acknowledges the financial support from the Swansea University, United Kingdom through the award of the Zienkiewicz scholarship. The finical support from the Sêr Cymru National Research Network is also appreciated.

References

[1] S. Zhou, J. Cao, D. J. Inman, Jing Lin, Shengsheng Liu, Zezhou Wang, Broadband tristable energy harvester: Modeling and experiment verification, Applied Energy, Volume 133, 2014, Pages 33-39, ISSN 0306-2619.

[2] S. Azizi, A. Ghodsi, H. Jafari, M. R. Ghazavi, A conceptual study on the dynamics of a piezoelectric MEMS (Micro Electro Mechanical System) energy harvester, Energy, Volume 96, 2016, Pages 495-506, ISSN 0360-5442.

[3] S. Wu, P.C.K. Luk, C. Li, X. Zhao, Z. Jiao, Y. Shang, An electromagnetic wearable 3-DoF resonance human body motion energy harvester using ferrofluid as a lubricant, Applied Energy, Volume 197, 1 July 2017, Pages 364-374.

[4] H. Madinei, H.H. Khodaparast, S. Adhikari, M.I. Friswell, M. Fazeli, Adaptive tuned piezoelectric MEMS vibration energy harvester using an electrostatic device Eur. Phys. J. Spec. Top., 224 (2015), pp. 2703-2717

[5] F. U. Khan and M. U. Qadir, State-of-the-art in vibration-based electrostatic energy harvesting, Journal of Micromechanics and Microengineering, Volume 26, 2016, Pages 103001.

[6] D. Zhao, C. Ji, C. Teo, S. Li, Performance of small-scale bladeless electromagnetic energy harvesters driven by water or air, Energy, Volume 74, 2014, Pages 99-108, ISSN 0360-5442.

[7] K. Fan, J. Chang, F. Chao, W. Pedrycz, Design and development of a multipurpose piezoelectric energy harvester, Energy Conversion and Management, Volume 96, 2015, Pages 430-439.

[8] S. Saadon, O. Sidek, A review of vibration-based MEMS piezoelectric energy harvesters, Energy Conversion and Management, Volume 52, Issue 1, 2011, Pages 500-504.

[9] X. Wang, C. Chen, N. Wang, H. San, Y. Yu, E. Halvorsen, X. Chen, A frequency and bandwidth tunable piezoelectric vibration energy harvester using multiple nonlinear techniques, Applied Energy, Volume 190, 15 March 2017, Pages 368-375.

[10] T. Yildirim, M. H. Ghayesh, Weihua Li, Gursel Alici, A review on performance enhancement techniques for ambient vibration energy harvesters, Renewable and Sustainable Energy Reviews, Volume 71, May 2017, Pages 435-449.

[11] R. Masana, M. F. Daqaq, Electromechanical Modeling and Nonlinear Analysis of Axially Loaded Energy Harvesters, Journal of Vibration and Acoustics, Volume 133, 2010, Pages 011007.

[12] V. R. Challa, M. G. Prasad, and F. T. Fisher, Towards an Autonomous Self-Tuning Vibration

Energy Harvesting Device for Wireless Sensor Network Applications, IOP Publishing, Smart Mater. Struct. 20 (2011) 025004.

[13] L. M. Miller, P. Pillatsch, E. Halvorsen, P. K. Wright, E. M.Yeatman, Andrew S. Holmes, Experimental passive self-tuning behavior of a beam resonator with sliding proof mass, Journal of Sound and Vibration 332, (2013) 7142.

[14] A. Erturk, D.J. Inman, Broadband piezoelectric power generation on high-energy orbits of the bistable Duffing oscillator with electromechanical coupling, Journal of Sound and Vibration, Volume 330, Issue 10, 2011, Pages 2339-2353.

[15] P.V. Malaji, Shaikh Faruque Ali, Broadband energy harvesting with mechanically coupled harvesters, Sensors and Actuators A: Physical, Volume 255, 1 March 2017, Pages 1-9.

[16] A. Alexeenko, S. Chigullapalli, J. Zeng, X. Guo, A. Kovacs and D. Peroulis, Uncertainty in microscale gas damping: Implications on dynamics of capacitive MEMS switches, Reliability Engineering and System Safety 96 (2011), pp. 1171–1183.

[17] N. Agarwal, N. Aluru, Stochastic modeling of coupled electromechanical interaction for uncertainty quantification in electrostatically actuated MEMS, Computer Methods in Applied Mechanics and Engineering, Vol. 197, Issue 43-44 (2008), pp. 3456–3471.

[18] N. Agarwal, N. Aluru, A data-driven stochastic collocation approach for uncertainty quantification in MEMS, International journal for Numerical Methods in Engineering, Vol. 83, Issue 5 (2010), pp. 575–597.

[19] A. Erturk, D.J. Inman, Piezoelectric Energy Harvesting, John Wiley & Sons, Chichester, UK, 2011.

[20] H. Madinei, G. Rezazadeh, S. Azizi, Stability and bifurcation analysis of an asymmetrically electrostatically actuated microbeam, J. Comput. Nonlinear Dyn. 10 (2) (2015) 021002.

[21] H. Madinei, H.H. Khodaparast, S. Adhikari, M.I. Friswell, Design of MEMS piezoelectric harvesters with electrostatically adjustable resonance frequency, Mech. Syst. Signal Process. 81 (2016) 360–374.

[22] M.I. Younis, MEMS Linear and Nonlinear Statics and Dynamics, vol. 20, Springer Science & Business Media, 2011.

[23] H. Madinei, H.H. Khodaparast, S. Adhikari, M.I. Friswell, Improving performance of MEMS piezoelectric harvesters in the presence of manufacturing uncertainties, International Conference on Uncertainty in Structural Dynamics (USD2016).

[24] E. Blokhina and D. Galayko, "Towards autonomous microscale systems: Progress in electrostatic kinetic energy harvesting," 2016 IEEE International Conference on Electronics,

Circuits and Systems (ICECS), Monte Carlo, 2016, pp. 744-747.